# Full-waveform inversion using a stepped-frequency GPR to characterize the tack coat in hot-mix asphalt (HMA) layers of flexible pavements

Amine Ihamouten, Frédéric Bosc, Borui Guan, Cédric Le Bastard, Cyrille Fauchard, Sébastien Lambot, Xavier Derobert

NDT & E international, Elsevier, 95 (2018), pp.17-25
http://dx.doi.org/10.1016/j.ndteint.2017.12.006

# Full-waveform inversion using a stepped-frequency GPR to characterize the tack coat in hot-mix asphalt (HMA) layers of flexible pavements

[1] Amine Ihamouten*, [1]Frédéric Bosc, [1,2]Borui Guan, [1]Cedric Le Bastard, [1]Cyrille Fauchard, [3]Sébastien Lambot and [2]Xavier Dérobert

*[1]CEREMA, DTO/DLRCA, URECND, Angers, France*
*[2]LUNAM Université, IFSTTAR, F-44340, Bouguenais, France*
*[3]Université catholique de Louvain (UCL), Belgium*

*corresponding author, e-mail address: amine.ihamouten@cerema.fr,
Cerema
49136, Les Ponts-de-Ce, France
tel: +33 2 41 79 13 28

Abstract

The use of tack coats in the construction of road structures is a technique that ensures pavement layer bonding. Unfortunately, existing techniques commonly used in France to estimate tack coat conditions require coring structures for *ad hoc* characterization in the laboratory. This paper investigates a non-destructive approach to characterize changes in geometric and dielectric properties of the tack coats present inside the hot-mix asphalt (HMA) layers of flexible pavements, with the use of a stepped-frequency radar combined with a mono-static, off-ground, ultra-wideband Vivaldi antenna. The principle of this method is to consider the flexible pavement as a multi-layered medium with changing properties (thicknesses, dielectric susceptibilities and dispersion parameters). Then a full-waveform inversion is applied, which allows for the extraction of the dielectric and geometric parameters of each layer composing the structure. Following numerical validations, the multi-layered forward model, namely, a Green's function model integrating the 2-parameter variant of Jonscher's model, combined with Lambot's *et al.* radar full-wave method was experimentally validated using calibrating media (up to three layered media). Then, the link between both the dielectric and the geometric parameters of the tack coats and the emulsion quantity (bonding) was analyzed. The results showed good agreement between measured and modeled radar data. Radar data inversions showed in particular that the dielectric susceptibility and thickness of the transition zone increase with the emulsion quantity. Future research will focus on the establishment of a reference database of calibration curves linking dielectric susceptibility and tack coat characteristics.

**Keywords:** *Stepped-frequency radar, Green's function, Jonscher's model, tack coat, pavements*.

## 1. INTRODUCTION

Bonding conditions at the interface between pavement layers (Figure 1) are known to modify the distribution of stresses and strains in flexible or rigid pavement structures and to influence their resistance to cyclic loading. Poor adhesion between layers can lead to premature degradation of the pavement, then to cracks. Although the tack coat technique is a common practice in road works in France, it is qualitatively poorly defined in terms of contractor obligations. Indeed, to this day, tack coats are only considered from a quantitative point of view in the linear setting, where the only homogeneity guarantee corresponds to the performance of the implementation machinery.

To better characterize these layers, various methods are under development or normalization. Thus, since Europe has undertaken standard works in the field of road building, some "Technical Specifications" have been proposed to deal with bonding tests in static and dynamic on asphalt cores (standards EN 12697-48 and TS 12697-51 [1, 2]). All these tests require on-site pavement coring, which presents several drawbacks. Indeed, in addition to limiting the diagnosis to restricted areas of the structure, coring imposes a prolonged exposure of operators to pollutants (asbestos, ionizing radiation, dust, etc.) and to the multiple hazards related to the worksites (road traffic, risks of collapses, reduced and unsecured accessibility, etc.). Limiting operator time on site is also an economic issue because it is to avoid infrastructure service outages in the transport domain.

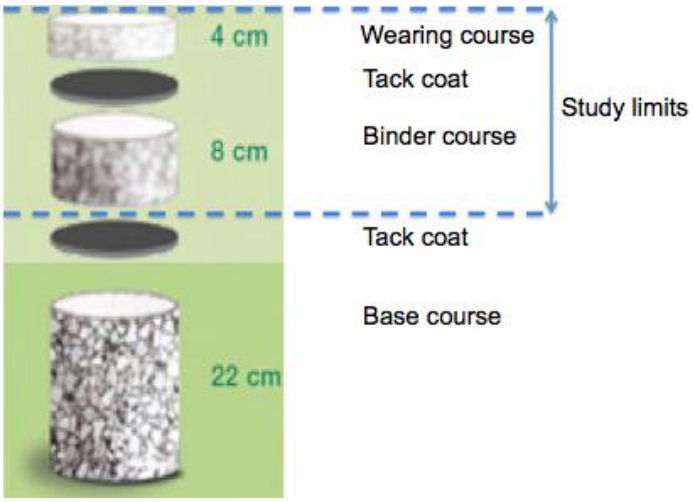


**Figure 1: Tack coat positioning in a pavement structure.**

Generally speaking, there are additional non-destructive (ND) or semi-destructive methods considered as references for the characterization of pavement layers in the laboratory and on-site (but not for tack coat characterization) that use gammadensimetry devices to estimate the density of road structures. Unfortunately, the restrictive legislation in many countries imposes ever stricter constraints on the storage, transportation and use of nuclear sources. Consequently, developing alternative techniques is a major concern for controlling newly-paved roads. The use of ND methods based on the propagation of electromagnetic (EM) waves represents an adequate solution to this problem.

Ground-penetrating radar (GPR) based on EM wave propagation, is a rising non-destructive technique for measuring the dielectric and geometric characteristics of materials. It is a common technique for geometrical applications (rebar detection [3, 4], road thickness estimation [5, 6], etc.) in civil engineering domain, and remains under study for material characterization (water and chloride content in concrete [7, 8], asphalt compaction [9, 10], etc.). Moreover, GPR techniques constitute a powerful tool for monitoring the condition of dispersive civil engineering materials. Wave propagation is entirely governed by the dielectric response, which reflects the interaction between propagating EM waves and the tested

material. Along these lines, several methods and models have been implemented, with varying degrees of success, in order to describe the frequency dependence of the dielectric permittivity of geological and civil engineering materials [11-17].

To estimate dielectric and geometric characteristics for civil engineering materials and multi-layered media, most researchers use the travel time delay (TTD) approach [18], which is limited in terms of forward modelling adequacy and information content. Full-waveform inversion (FWFI), which is based on an accurate forward model and an inversion method, has demonstrated to be a powerful technique for material characterization [11, 12, 19, 20]. Although air-coupled GPR has been more often used in FWFI compared to the more complex ground-coupled GPR configurations [11, 21], ground-coupled GPR can now be accurately modeled as well [12, 22]. Ground-coupled GPR permits deeper characterization and finer resolution compared to air-coupled radars.

The general objective of this paper is to investigate FWFI of radar waves to remotely estimate both the dielectric and geometric properties of tack coats in pavement structures based on the full-wave radar method of Lambot *et al.* [11, 12, 22] (patented) combined with Jonscher's model of frequency-dependent medium properties. The adopted approach was validated in the laboratory on a wide range of materials and pavement layers representing a sample of existing road structures in France. From a durability point of view, this work aimed at demonstrating (before quantifying) the relationship between ND observables (permittivity, susceptibility, dispersion parameter, etc.) and the emulsion quantities used in the bonding of pavement layers. Concerning this main objective, three specific scientific issues were addressed in this paper: (1) Establishment of a laboratory experimental design including a significant number of controlled specimens (various emulsion quantities, thicknesses, etc.) intended for dielectric and geometric characterization with a Stepped-Frequency Radar - SFR (Section II); (2) Validation of the forward approach integrating the 2-parameter variant of

Jonscher's model on numerical data (Sections III); and (3) SFR data processing on samples in the laboratory to link dielectric characteristics with emulsion quantities for various specimens (Section IV).

## 2. Phenomenological aspects and experimental design

In this study, we focused solely on tack coats linking the wearing course and the binder course (Figure 1). We developed a SFR that integrates a PC-piloted FieldFox Microwave vector network analyzer (Agilent N9928A) and various Vivaldi antennas in mono-static, near-field configuration (Figure 2) for measuring a wide range of HMA layers (slabs). The details of this experimental device are presented in Section IV. A preliminary study was performed to assess the sensitivity of such a device (using its raw data expressed in the time domain) to the presence or absence of tack coat emulsion. To do this, 2 two-layer slabs were designed. The first one did not contain any emulsion at the interface between the wearing course (BBTM - 3 cm thick HMA corresponding to very thin layers) and the binder course (BBSG - 6 cm thick). The second contained emulsion up to 600 g/m$^2$. Figure 3 shows the time variations of the real part of the SFR reflection coefficients $S_{11}$ on the slabs, laid on a Perfect Electrical Conductor (PEC), with (blue curve) and without (red curve) emulsion.

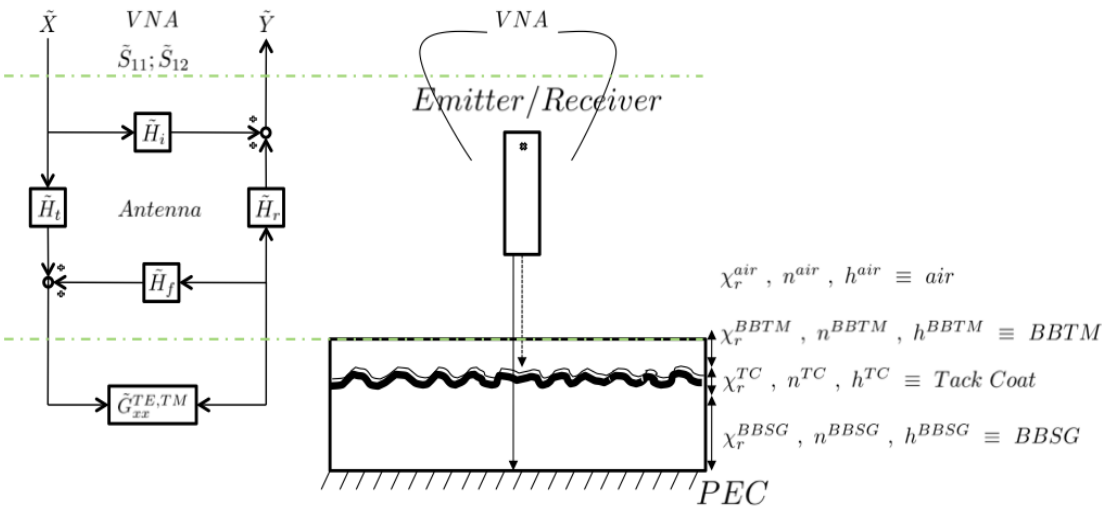


**Figure 2: SFR schematic modeling diagram [11, 12, 22] and experimental setup.**

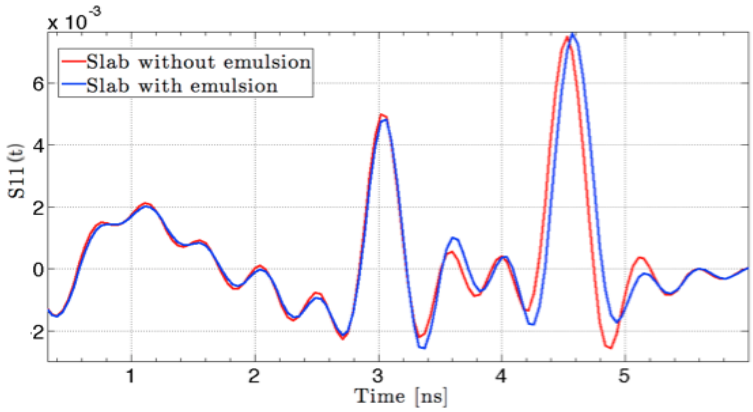


**Figure 3: Time signals through similar slabs without (red line) and with (blue line) emulsion.**

The presence of emulsion at the BBTM / BBSG interface decreased the wave propagation velocity, implying a time delay in the second echo corresponding to reflection at the bottom of the slabs (BBSG/PEC). This phenomenon is explained by the fact that the emulsion filled the empty pores at the BBTM/BBSG interface, compared to an air gap, which increases the dielectric permittivity of the transition zone between the two layers. This transition zone is also visible in the gammadensimetry results (Figure 4).

As a reminder **[23]**, the gammadensimetry method is based on the absorption of gamma photons emitted by a radioactive source of Cesium C137 S, with energy 0.662 MeV, after passing through the material. This absorption follows Lambert's law:

$$N = N_o \exp(-z\mu_0 \rho x), \qquad (1)$$

where $N_o$ is the number of incident photons and $N$ is the number (in counts per second) of collected photons, $\mu_0$ (cm$^2$/g) is the mass absorption coefficient of the tested material, $\rho$ (g/cm$^3$) is the density, $x$ the thickness of the material and $z$ is the correction coefficient defined by the geometry of the device. The density can therefore be given by the equation:

$$\rho = -\frac{1}{z\mu_0 x} ln\left(\frac{N_0}{N}\right), \qquad (2)$$

Knowing $z$, $\mu_0$ and the thickness of the material $x$ makes it possible to calculate the density $\rho$.

The result of these gammadensimetry measurements is of major importance to the developed FWFI that aims to invert the parameters of the transition zone (i) considered in the presented approach as a dielectric layer in the forward model, and (ii) whose dielectric properties are directly proportional to emulsion quantity. Thus, to establish the link between the emulsion quantity used in the tack coat and the dielectric characteristics derived from SFR measurements, 32 two-layer slabs (three-layers if we consider the transition zone as a layer) were designed and built. To reach 64 samples, the 32 slabs were upturned during the SFR measurements.

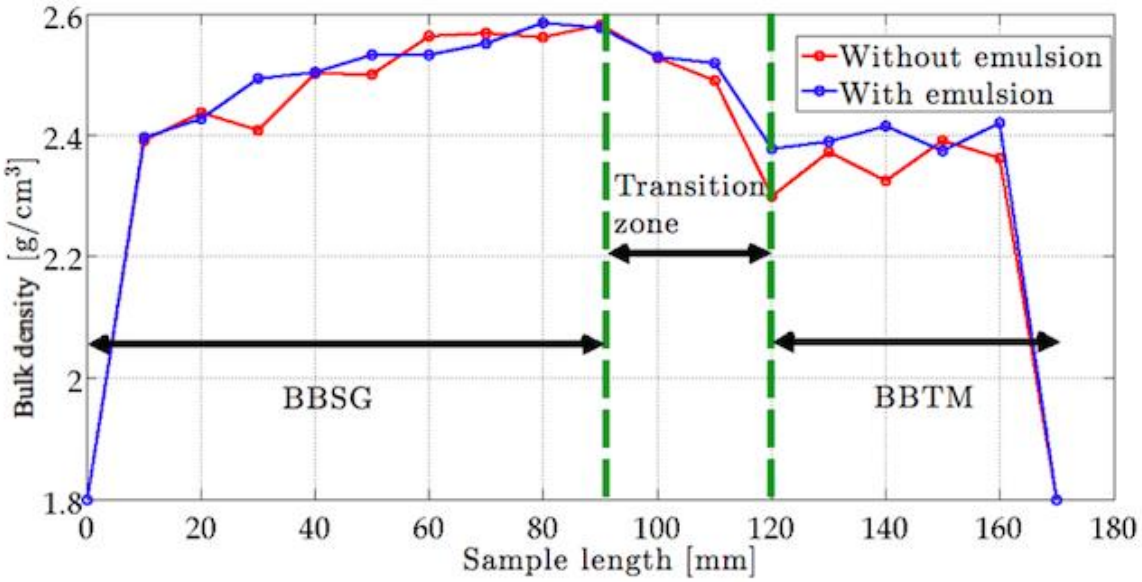


**Figure 4: Bulk density variations according to slab thickness with and without emulsion.**

156 The HMA layer nomenclature used in the experimental design is as follows:

157 • BBTM – Very thin bituminous concrete: the target average thickness ranges from 2 to
158 2.5 cm. The binder content is 5.5% and the aggregate size fraction is 0/10 mm with a
159 discontinuity between 2 mm and 6 mm;

160 • BBSG – Semi-coarse HMA: used for surface layers (wearing and/or binder courses) in
161 roadways with medium to high traffic. The target average thickness ranges from 5.5 to 6 cm,
162 the binder content is 5.2% and the aggregate size fraction is 0/10 mm;

163 • GB – bituminous gravel used for the base course. The target average thickness ranges
164 from 10.5 to 11.5 cm, the binder content is 4% and the aggregate size fraction is 0/14 mm.

165 The 4 degrees of freedom for this statistic experimental design are as follows: emulsion
166 quantity (0, 200, 400 and 600 g/m$^2$), nature of the layers (BBTM above BBSG and BBSG
167 above GB), their thicknesses (BBTM / 3cm, BBSG / 6cm and GB / 11cm) and their
168 compaction (between 75% and 96%) (Table 1).

169 Two aggregate mineralogical types (Diorite and Gneiss) from two different quarries (Noubleau
170 - N and Le Tronc - LT) were used in order to have two different dielectric permittivities for
171 aggregates (between 5 and 7 for diorite and between 8 and 15 for gneiss).

172 Calibration slabs were also carried out for each layer of the experimental design necessary to
173 initialize the FWFI procedure (allowing the determination of dielectric characteristics of
174 BBTM, BBSG and GB layers considering their thicknesses).

175 With respect to manufacturing, all samples were made in the laboratory using the MLPC plate
176 compactor and the RETEX texture reproduction module with compaction verification by
177 gammadensimetry measurements.

178

179 **Table 1: Experimental design characteristics.**

| Samples | Lower layer (upturned = Upper layer) | Upper layer (upturned = Lower layer) | Emulsion quantity | Manufacturing date |
|---|---|---|---|---|
| **Ech1** | BBSG10 LT[(1)] C91[(2)] | BBTM10 N[(3)] C75 | 200 g/m² | 14/11/14 |
| **Ech2** | BBSG10 LT C96 | BBTM10 N C75 | 200 g/m² | 17/12/14 |
| **Ech3** | BBSG10 LT C91 | BBTM10 N C90 | 200 g/m² | 03/03/15 |
| **Ech4** | BBSG10 LT C96 | BBTM10 N C90 | 200 g/m² | 04/12/14 |
| **Ech5** | GB14 N C88 | BBSG10 LT C91 | 200 g/m² | 2016-2017 |
| **Ech6** | GB14 N C96 | BBSG10 LT C91 | 200 g/m² | 2016-2017 |
| **Ech7** | GB14 N C88 | BBSG10 LT C96 | 200 g/m² | 2016-2017 |
| **Ech8** | GB14 N C96 | BBSG10 LT C96 | 200 g/m² | 2016-2017 |
| **Ech9** | BBSG10 LT C91 | BBTM10 N C75 | 600 g/m² | 25/11/14 |
| **Ech10** | BBSG10 LT C96 | BBTM10 N C75 | 600 g/m² | 07/01/15 |
| **Ech11** | BBSG10 LT C91 | BBTM10 N C90 | 600 g/m² | 27/03/15 |
| **Ech12** | BBSG10 LT C96 | BBTM10 N C90 | 600 g/m² | 11/12/14 |
| **Ech13** | GB14 N C88 | BBSG10 LT C91 | 600 g/m² | 2016-2017 |
| **Ech14** | GB14 N C96 | BBSG10 LT C91 | 600 g/m² | 2016-2017 |
| **Ech15** | GB14 N C88 | BBSG10 LT C96 | 600 g/m² | 2016-2017 |
| **Ech16** | GB14 N C96 | BBSG10 LT C96 | 600 g/m² | 2016-2017 |
| **Ech17** | BBSG10 LT C91 | BBTM10 N C75 | 0 g/m² | 06/11/14 |
| **Ech18** | BBSG10 LT C96 | BBTM10 N C75 | 0 g/m² | 16/12/14 |
| **Ech19** | BBSG10 LT C91 | BBTM10 N C90 | 0 g/m² | 27/01/15 |
| **Ech20** | BBSG10 LT C96 | BBTM10 N C90 | 0 g/m² | 02/12/14 |
| **Ech21** | GB14 N C88 | BBSG10 LT C91 | 0 g/m² | 2016-2017 |
| **Ech22** | GB14 N C96 | BBSG10 LT C91 | 0 g/m² | 2016-2017 |
| **Ech23** | GB14 N C88 | BBSG10 LT C96 | 0 g/m² | 2016-2017 |
| **Ech24** | GB14 N C96 | BBSG10 LT C96 | 0 g/m² | 2016-2017 |
| **Ech25** | BBSG10 LT C91 | BBTM10 N C75 | 400 g/m² | 21/11/14 |
| **Ech26** | BBSG10 LT C96 | BBTM10 N C75 | 400 g/m² | 06/01/15 |
| **Ech27** | BBSG10 LT C91 | BBTM10 N C90 | 400 g/m² | 06/03/15 |
| **Ech28** | BBSG10 LT C96 | BBTM10 N C90 | 400 g/m² | 10/12/14 |
| **Ech29** | GB14 N C88 | BBSG10 LT C91 | 400 g/m² | 2016-2017 |
| **Ech30** | GB14 N C96 | BBSG10 LT C91 | 400 g/m² | 2016-2017 |
| **Ech31** | GB14 N C88 | BBSG10 LT C96 | 400 g/m² | 2016-2017 |
| **Ech32** | GB14 N C96 | BBSG10 LT C96 | 400 g/m² | 2016-2017 |

180 [(1)]LT = Le Tronc quarry, [(2)] C91 = Compaction at 91%, [(3)]N = Noubleau quarry

181 In the context of this paper, we focused only on four series for a total of 32 slabs (BBTM /
182 BBSG and BBSG / BBTM) with the four emulsion quantities (total of 16 slabs that we
183 upturned).

Slab size was determined from a parametric study (not detailed in this paper) associated with the radiation pattern of the Vivaldi antenna used in order to avoid edge effects that are not included in the forward model, which assumes infinite horizontal layers.

## 3. EM WAVE PROPAGATION MODEL

The aim of this section is to present the fast calculation time model describing an air-coupled radar wave propagation through multi-layered media, taking into account the frequency-dependence of electromagnetic properties. As shown in the Figure 2, this problem can be described as EM wave propagation through a three-layer planar and lossless medium (BBTM/Tack coat/BBSG). The considered transceiver (emitter/receiver) simulates a mono-static stepped-frequency radar, giving high effective bandwidth with plural narrow instantaneous bandwidth.

Lambot *et al*. [11] proposed a closed-form, intrinsic antenna model combined with zero-offset Green's function to describe radar propagation in planar-layered media. This model holds when the distribution of the backscattered field over the antenna aperture is constant, which in particular occurs in far-field conditions (homogeneous field in that later case). Afterwards, this antenna model was generalized to near-field conditions [12, 22], for which the field distribution over the antenna aperture is variable. In that case, multi-offset Green's functions are used. Furthermore, both a linear model and Debye's model were used by the authors to describe the frequency dependence of dielectric permittivity of dispersive materials. However, a previous study [24] showed the advantages of using a two-parameter (2p) variant of Jonscher's model [25], which has proven its efficiency in describing the dielectric response of civil engineering materials with a constant quality factor *Q*. Therefore, in this paper, we used this Jonscher's model with a limited number of parameters (2) to describe the frequency dependence of the material EM properties.

In the following sub-sections, the theoretical Jonscher's model is reminded. It describes the frequency dependence of the effective permittivity by means of 2 parameters, susceptibility and loss exponent. The model of Lambot *et al*. [11, 12, 22] is then applied to relate the total return loss $S_{11}$ to Jonscher's parameters and is parameterized with a single point source and receiver, which provides sufficient accuracy for our model configuration [20] (the antenna is at sufficient distance from the medium). The overall model is numerically studied and then experimentally validated in the next sections.

### 3.1. **Effective permittivity**

The effective permittivity is a complex and frequency-dependent quantity in dispersive materials. The 2p variant of Jonscher's model is chosen instead of the universal model because the association BBTM / Tack Coat / BBSG is considered as a *Q*-constant dielectric medium, thereby reducing the number of unknown parameters by two over the whole frequency band.

Jonscher's model is based on universality in the form of dielectric response. The model states that, above the peak loss, should one exist, the dielectric susceptibility $\chi = \chi' - \mathrm{j}\chi''$ of all dielectric systems follows a frequency power law $\chi'(\mathrm{f}) \propto \chi''(\mathrm{f}) \propto \mathrm{f}^{\mathrm{n}-1}$ where $f$ is the frequency and $n$ a parameter ranging from 0 to 1. The dielectric susceptibility can be defined as a quantity characterizing the capability of a material to be polarized. Quantitatively, it equals the proportionality coefficient relying the intensity of the applied electric field and the polarization of the material (the dipole moment per unit volume of the dielectric). Generally speaking, the dielectric properties of a material are characterized by dielectric susceptibility, as well as by its dielectric permittivity.

The effective permittivity can be expressed as follows:

$$\varepsilon_e = \varepsilon_o \chi_r \left(\frac{f}{f_r}\right)^{n-1} \left(1 - jcot\left(\frac{n\pi}{2}\right)\right), \qquad (3)$$

where $\chi_r$ is the reference susceptibility, $n$ is the loss exponent, $\varepsilon_o$ is the permittivity of vacuum and $f_r$ is the reference frequency arbitrarily chosen.

### 3.2. **Green's function**

The planar multi-layered medium Green's function in the frequency and spectral domains is calculated for the one-point source-receiver using (4).

$$G(\kappa) = \frac{1}{8\pi}\left(\frac{\gamma_1 R_1^{TM}}{j\omega\varepsilon_{e1}} - \frac{j\omega\mu_1 R_1^{TE}}{\gamma_1}\right) e^{-2\gamma_1 h_1} \qquad (4)$$

In this equation, $\omega$ is the angular frequency; subscript 1 refers to the upper half-space (free-space); $h_1$ is the distance between transceiver points and the first material interface; $R_1^{TM}$ and $R_1^{TE}$ are respectively the transverse magnetic (TM) and transverse electric (TE) global reflection coefficients concerning all reflections in layered material; $\gamma_1$ is the complex vertical wavenumber defined as $\gamma_1 = \sqrt{\kappa^2 - j\omega\mu_1\eta_1}$, where $\mu_1$ and $\eta_1$ are, respectively, the magnetic permeability and complex conductivity of air. The spatial-domain Green's function is obtained from its spectral counterpart using Sommerfeld's integration [26].

### 3.3. **Return loss $S_{11}$**

Return loss $S_{11}$, the output of the radar equation, is the ratio of reflected and emitted EM electric fields. Assuming a single point source and receiver as approximation to describe our near-field radar data, it is defined by the following equation [12, 22]:

$$S_{11}(f) = R_i(f) + T_s(f)\big(1 - G(f)R_s(f)\big)^{-1} G(f)T_i(f) \qquad (5)$$

where, $R_i$ is the free space response of the antenna. $T_i$ and $T_s$ are the global transmission coefficients of the antenna for fields incident from the radar reference plane onto the source point and vice-versa, $R_S$ is the global reflection coefficient for fields incident from the field point onto the radar reference plane, and $G$ is the spatial domain Green's function, deduced from the spectral domain Green's function in (4).

The transmission and reflection coefficients are determined by solving equations (6-8) for two near-field measurements on a PEC with two different antenna heights $S_{pec3}$ and $S_{pec5}$ (3 cm and 5 cm), by measuring the open-air impedance $S_{air}$, and by calculating the corresponding Green's functions $G_{pec3}$ and $G_{pec5}$ for these two antenna heights [11].

$$R_i = S_{air} \quad (6)$$

$$R_s = \frac{\frac{S_{pec5}-S_{air}}{G_{pec5}} - \frac{S_{pec3}-S_{air}}{G_{pec3}}}{S_{pec5}-S_{pec3}} \quad (7)$$

$$TiTs = \frac{S_{pec5}-S_{air}}{G_{pec5}} - (S_{pec5} - S_{air})R_s \quad (8)$$

Once the global transmission and reflection coefficients $(R_i, T_iT_s, R_s)$ are determined, the return loss $S_{11}$ is directly calculated using the zero-offset, single-point Green's function. It is worth noting that these antenna transfer functions may be slightly different from those which would be obtained in farer conditions, but they correspond to the field distribution over the antenna aperture occurring in that height range [20, 27].

### 3.4. **Inversion objective function**

Given the analytical forward model, EM wave propagation through the radar-antenna-layered medium is described. However, we need to solve the inverse problem. The objective of inversion is to have the best group of model parameters that minimizes the difference between analytical $S_{11}$ and reference (numerical or experimental) $S_{11}$, assuming that this group of parameters to correspond to the right configuration.

There are three main kinds of inversion methods. FWFI reliability has been well demonstrated [11, 12, 19, 20]. As time gating was not necessary in our study, we performed inversion in the frequency domain in order to avoid the inverse Fourier transform calculation, and hence, minimize processing time.

The amplitude-weighted average distance between analytical and reference return loss $S_{11}$ complex values at each frequency was considered as objective function (9).

$$O(m) = \frac{1}{NF}\sum_{i=1}^{NF}\frac{|S_{mod}(f_i,m)-S_{ref}(f_i,m)|}{|S_{ref}(f_i,m)|} \quad (9)$$

Here, $S_{mod}(f_i, m)$ and $S_{ref}(f_i, m)$ are the analytical and reference return loss $S_{11}$ at the frequency $f_i$. $m$ corresponds to the model parameter vector. *NF* is the number of frequencies. There is a return value $O(m)$ for each try of model parameter. The best parameter is reached once $O(m)$ is minimized using genetic algorithm.

## 4. NUMERICAL VERIFICATION OF THE FORWARD MODEL

High Frequency Electromagnetic Field Simulation (HFSS) is a commercial electromagnetic simulation software based on the finite element method. The aim of this section is to present an HFSS-based numerical verification approach, in order to evaluate the stability and robustness of our analytical model when estimating the dielectric and geometric characteristics of a multi-layered medium representing road structures with a tack coat equivalent layer.

Thus, a Vivaldi ultra-wideband antenna was designed and activated from 0.8 to 3 GHz with a frequency step of 5 MHz. The phase center of this antenna was fixed at a distance of 10.53 cm inward from its aperture. Following the procedure described in Section 3.3, we performed the calibration process to obtain the global, frequency-dependent transmission and reflection coefficients of the antenna.

The model configuration is shown in Figure 5. The height of the antenna (distance between the antenna aperture and the upper surface of the BBTM layer) was set to 4 cm, meaning a near-field case simulation [26]. The thickness, the dielectric susceptibility and the loss exponent for each layer are reported in Figure 5, considering that they are used as inputs for both numerical and analytical models.

Figures 6 and 7 correspond to examples of time and frequency variations of the real parts of the HFSS Green's functions (red curves) and those of our model including the 2p variant of Jonscher's model (blue curves).

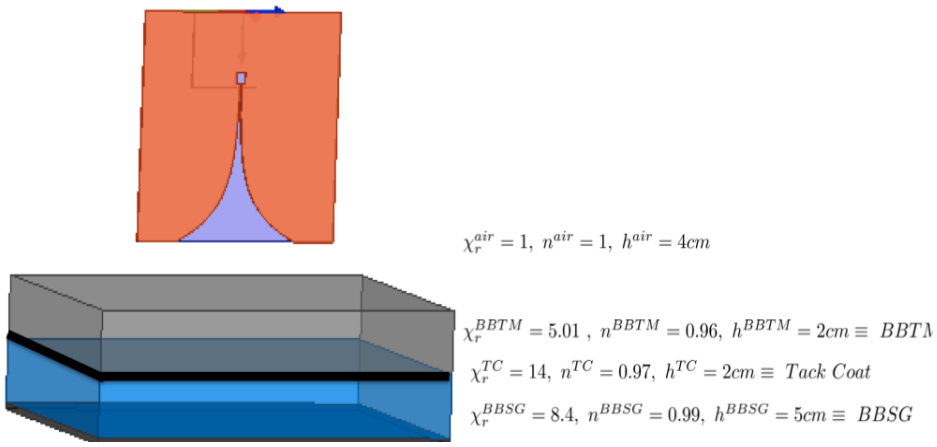


**Figure 5: HFSS- based numerical model.**

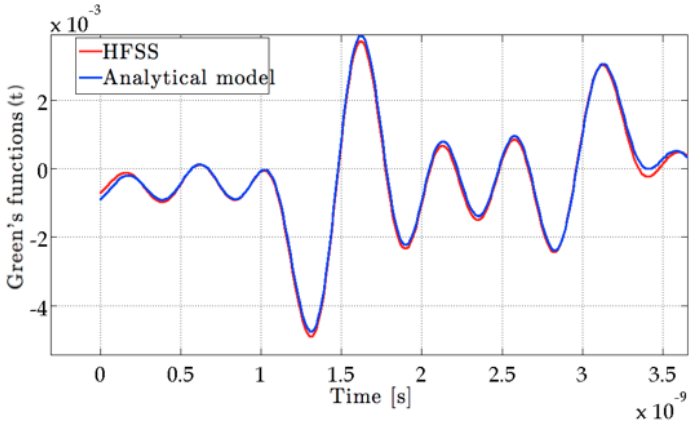


**Figure 6: Time variation of the real parts of the HFSS Green's functions (red curve) and of the analytical model (blue curve) after the numerical calibration process.**

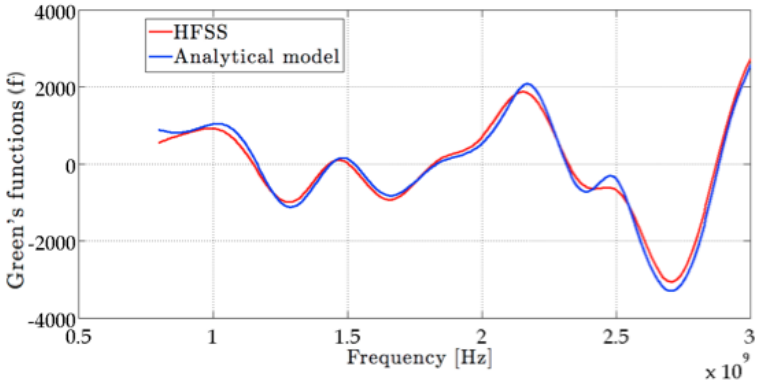


**Figure 7: Frequency variation of the real parts of the HFSS Green's functions (red curve) and of the analytical model (blue curve) after the numerical calibration process.**

The values of the Green's analytical model integrating 2p variant of Jonscher's model perfectly match the reference theoretical values (HFSS) after the near-field calibration of the

antenna. The small differences between the two model curves are partly due to the single point source and receiver approximation for this near-field configuration (the field distribution over the antenna aperture slightly changes between 3 and 5 cm height).

Thus, a generalization of this numerical study (not completely presented in this paper) allowed us to validate the forward and inverse procedures before the transition to the experimental study.

## 5. EXPERIMENTAL VALIDATION

A wide characterization experiment was carried out in order to test our method for estimating the tack coat characteristics. The SFR system consists of a PC-piloted FieldFox Microwave vector network analyzer (Agilent N9928A) connected to the Vivaldi antenna [28], in order to setup the ultra-wideband (UWB), stepped-frequency continuous-wave (SFCW) radar system. The scattering parameters were measured at the VNA reference calibration plane, located at the cable connector to which the antenna is connected. In a mono-static configuration, the frequency-dependent, complex return loss $S_{11}$ from the VNA in the range 0.8 to 3 GHz is the measured variable. Following the procedure described in Section 3.3, the system was calibrated to obtain the antenna transmission and reflection coefficients.

Additionally, fine characterization was carried out in an anechoic chamber in order (i) to determine the radiation pattern of the Vivaldi antenna and (ii) to assess the edge effects that are generated by the samples with a limited size and not considered in the proposed model (Figures 8 and 9).

The first SFR measurements were performed on two series of four BBTM / tack coat / BBSG slabs (dimensions 40 cm × 30 cm × 9.5 cm) placed on a metal plate of similar dimensions. The SFR measurement configuration is shown in Figure 10, wherein the Vivaldi

antenna is placed 4 cm above the slabs. It should be noted that the rear aerial EM echoes from the metallic antenna-holder are accounted for by the antenna calibration process.

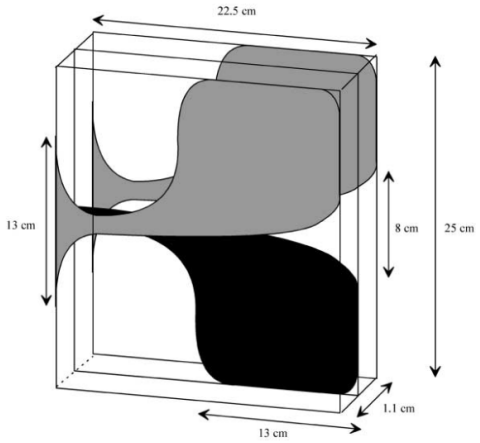


**Figure 8: Structure of the Vivaldi antenna [28].**

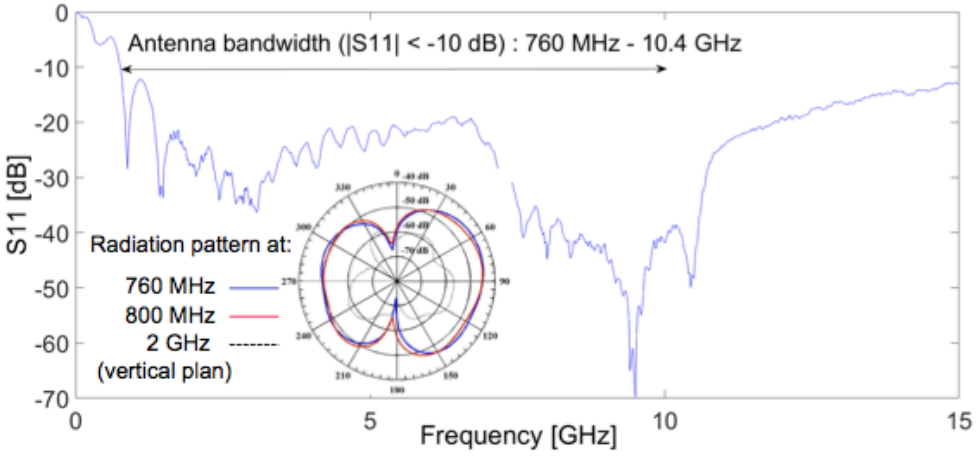


**Figure 9: Vivaldi antenna radiation pattern and free space response.**

**Figure 10: Experimental setup.**

The global inversion calculation is initialized with the parameters $\chi r_{BBTM}$, $n_{BBTM}$, $\chi r_{BBSG}$ and $n_{BBSG}$ determined from a first inversion procedure of SFR measurements made on the calibration slabs (dimensions 40 cm × 30 cm × 3 cm for BBTM and 40 × 30 cm × 5 cm for BBSG).

Figures 11 and 12 correspond to examples of time and frequency variations of the real parts of the experimental Green's functions (red curves) and those of our model including the 2p variant of Jonscher's model (blue curves) in the case of a tack coat (between BBTM and BBSG layers) with an emulsion quantity equal to 600 g/m$^2$.

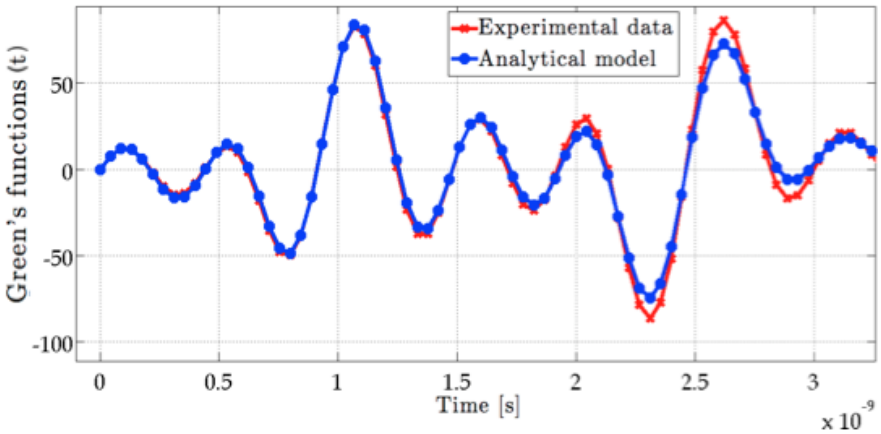


**Figure 9: Time variation of the real parts of the experimental Green's functions (red curve) and of the analytical model (blue curve) after the experimental calibration process.**

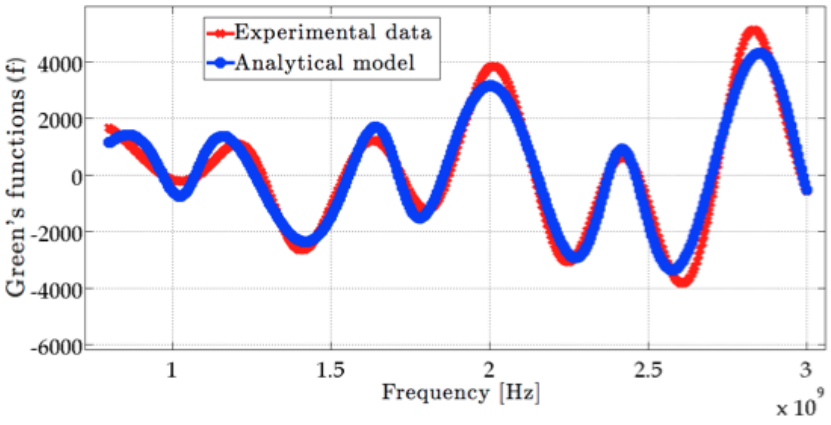


**Figure 10: Frequency variation of the real parts of the experimental Green's functions (red curve) and of the analytical model (blue curve) after the experimental calibration process.**

These results show a relatively good agreement between the analytical model and experimental data. Thus, all inversion results representing these two series (BBTM / Tack coat / BBSG) are reported in Table 2.

These results lead to the following remarks:

- the greater the emulsion quantity, the higher the dielectric susceptibility of the transition zone. This confirms the results of the preliminary study in Section 2,
- the greater the emulsion quantity, the thicker the transition zone in contrast to BBTM thickness.

**Table 2: Full waveform inversion results**

| **Sample number** | **Emulsion quantity ($g/m^2$)** | $h^{inv.}_{BBTM}$ **(mm)** | $h^{inv.}_{TC}$ **(mm)** | $h^{inv.}_{BBSG}$ **(mm)** | $\chi_{r_{TC}}^{inv.}$ **(-)** | $n_{TC}^{inv.}$ **(-)** |
|---|---|---|---|---|---|---|
| **17** | 0 | 32.2 | 12.1 | 61.4 | 4.27 | 0.98 |
| **1** | 200 | 30.9 | 12.7 | 64.9 | 4.35 | 0.99 |
| **25** | 400 | 27.8 | 13.9 | 66.6 | 4.72 | 0.99 |
| **9** | 600 | 27.1 | 14.7 | 68.1 | 5.01 | 0.99 |
| **20** | 0 | 29.3 | 11.3 | 65.3 | 4.21 | 0.97 |
| **4** | 200 | 27.8 | 12.4 | 67.2 | 4.35 | 0.99 |
| **28** | 400 | 27.2 | 12.1 | 65.1 | 4.74 | 0.98 |
| **12** | 600 | 26.1 | 13.8 | 66.2 | 4.98 | 0.99 |
| **19** | 0 | 30.5 | 11.7 | 63.7 | 4.38 | 0.99 |
| **3** | 200 | 27.1 | 13.8 | 68.4 | 4.92 | 0.99 |
| **27** | 400 | 26.9 | 13.1 | 67.5 | 4.74 | 0.99 |
| **11** | 600 | 25.9 | 14.5 | 67.8 | 5.03 | 0.99 |
| **18** | 0 | 33.8 | 13.9 | 57.3 | 4.22 | 0.98 |
| **2** | 200 | 30.1 | 15.8 | 63.8 | 4.23 | 0.99 |
| **26** | 400 | 25.9 | 12.7 | 67.8 | 4.45 | 0.99 |
| **10** | 600 | 24.8 | 12.8 | 68.2 | 4.89 | 0.99 |

The presence of some outliers in these results (*i.e.*, sample 3) can be partly explained by the residues of the single point source and receiver approximation for this near-field configuration that does not take into account the changes in the field distribution over the antenna aperture. The second assumption for the origin of these outliers is related to the roughness of the

objective function showing a convergence to local minima and the need to use a more time-consuming specific iterative algorithm with more generations.

The results of this experimental study prove that this analytical model is suitable for describing SFR wave propagation through multi-layered media with a correlation between dielectric susceptibility and emulsion quantity. Thus, the future objective will be to generalize this study to a more complete experimental design for obtaining laboratory calibration curves that will link the ND observable $\chi_{r_{TC}}$ to the durability indicator (emulsion quantity).

## 6. Conclusion

A model of stepped-frequency radar wave propagation through HMA layers of flexible pavements was investigated using both numerical and experimental experiments. The FWFI was tested in near-field conditions for estimating the dielectric and geometric characteristics of a wide range of materials and pavement layers. In particular, we used a homemade ND technique based on a vector network analyzer combined with a homemade Vivaldi antenna (stepped frequency radar), associated with the radar model and methods of Lambot *et al.* [11, 12, 22] combined with Jonscher's parameterization for describing the frequency-dependent medium properties. This first step durability process demonstrated the relationship between ND observables (dielectric susceptibility) and the emulsion quantities used in the pavement layer bonding process.

Experimental results show a monotone evolution of the emulsion quantity according to the estimated dielectric susceptibility of the transition zone. This tendency is explained by the fact that the emulsion filled the empty pores at the interface, compared to an air gap, which increases the dielectric permittivity of the transition zone between the two layers. This transition zone is also visible in the gammadensimetry results.

Moreover, we noted that the emulsion quantity has an influence on the estimated layer thicknesses. Indeed, the greater the emulsion quantity, the thicker the transition zone in contrast to BBTM thickness.

Concerning the inverse problem, the presence of outliers in the FWFI results can be partly explained by the residues of the single point source and receiver approximation for this near-field configuration that does not take into account the changes in the field distribution over the antenna aperture. For the next step of this research work, we propose that an equivalent Green's function model can be built to describe the border effects and a multi-dipoles Green function model in a simple mathematical form can replace the current single-dipole Green function model to include more accurately the near-field effects.

The second assumption for the origin of these outliers is related to the roughness of the objective function showing a convergence to local minima and the need to use a more time-consuming specific iterative algorithm. An optimization of the objective function can be studied and proposed in the future in order to improve the performance of the inversion method. The genetic algorithm method can be combined with other local minimization method, in order to make a balance between the inversion result performances and the inversion time costs.

Generally speaking, the results of these preliminary research works prove that the FWFI approach combined to SFR technique is suitable for describing wave propagation through multi-layered media with a correlation between dielectric susceptibility and emulsion quantity. Thus, the future objective will be to generalize this study to a more complete experimental design for obtaining laboratory calibration curves that will link the ND observable $\chi_{r_{TC}}$ to the durability indicator (emulsion quantity). This second inverse problem will be solved statistically by applying a non-deterministic optimization (machine learning) algorithm to the

436 in-lab calibration curves that tie the controlled tack coats in various hot mix asphalt layers with
437 the dielectric susceptibility output by the laboratory EM characterization device.

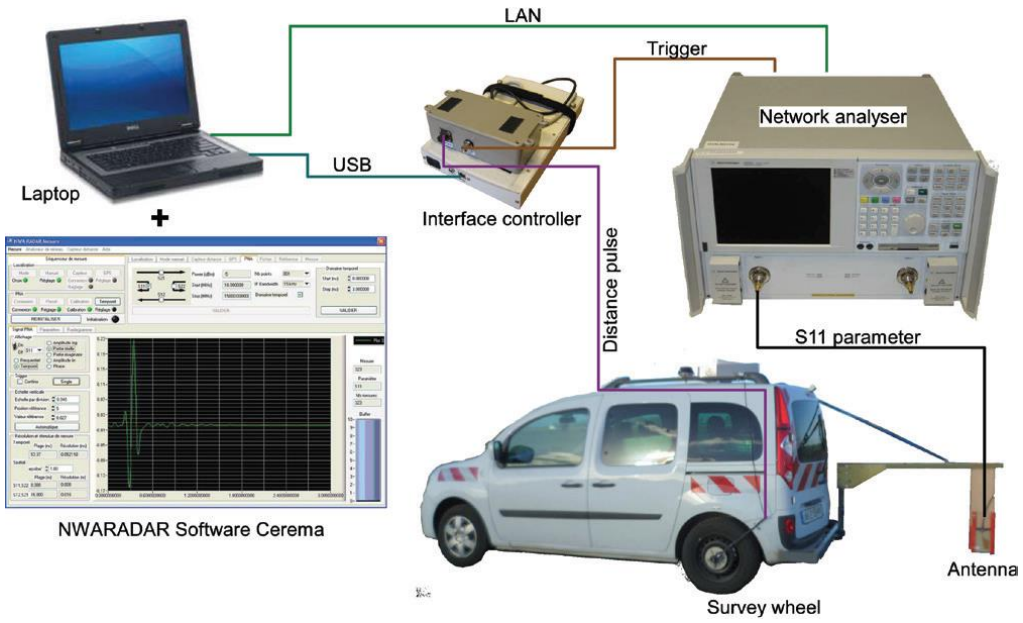


438
439

**Figure 11: Stepped Frequency Radar system of Cerema for road survey.**

440

441 Finally, we have already begun the phase of *in situ* deployment of this non-destructive tool
442 (Figure 11) in collaboration with the Vendée Departmental Council (France). The objective is
443 to classify the bonding areas into three categories on a new roadway (basing on test data bases
444 of the machine learning method that uses the in-lab validated kernels). Indeed, the
445 infrastructure owner has made a test area with three partial sections (30 m) oversized in terms
446 of emulsion quantity (600 and 800 g/m$^2$) into a global section (2.5 km) with a usual dosage of
447 400 g/m$^2$. At the roadway time zero state (without loading due to traffic), our initial right
448 classification rate was around 70% on all the inverted signals using the current and the small
449 training data base (incomplete and preliminary test). This structure is still considered as an *in*
450 *situ* validation area for our approach. The idea is to integrate in the future works additional
451 structural constraints and evaluate accordingly the accuracy of our SFR device and the stability
452 of our inverse methods.

## 7. REFERENCES


[1]. Standard EN 12697-48:2014 Bituminous Mixtures - Test Methods For Hot Mix Asphalt - Part 48: Interlayer Bonding. French standard association (AFNOR)

[2]. Standard UNI CEN/TS 12697-51:2017 Bituminous mixtures - Test methods - Part 51: Surface shear strength test. UNI standard

[3]. F. Soldovieri, R. Persico, E. Utsi, V. Utsi, The application of inverse scattering techniques with ground penetrating radar to the problem of rebar location in concrete, NDT & E International, Volume 39, Issue 7, October 2006, Pages 602-607, ISSN 0963-8695

[4]. V. Utsi, E. Utsi, Measurement of reinforcement bar depths and diameters in concrete. In: E. Slob, A. Yarovoy, J. Rhebergen, editors. Proceedings of the tenth international conference on ground penetrating radar. The Netherlands: Delft; 2004. p. 658–62

[5]. A. Benedetto, F. Tosti, L.B. Ciampoli, F. D'Amico, An overview of ground-penetrating radar signal processing techniques for road inspections, Signal Processing, Available online 18 May 2016, ISSN 0165-1684

[6]. D. Daniels, Ground Penetrating Radar. Inspec/IEE, 30 October 2004, ISBN: 0863413609

[7]. S.F. Senin, R. Hamid, Ground penetrating radar wave attenuation models for estimation of moisture and chloride content in concrete slab, Construction and Building Materials, Volume 106, 1 March 2016, Pages 659-669, ISSN 0950-0618

[8]. J. Huggenschmidt, R. Loser, Detection of chlorides and moisture in concrete structures with ground penetrating radar. Materials and Structures (2008) 41:785–792

[9]. D.H. Chen, F. Hong, W. Zhou, P. Ying, Estimating the hotmix asphalt air voids from ground penetrating radar, NDT & E International, Volume 68, December 2014, Pages 120-127, ISSN 0963-8695

[10]. C. Fauchard, B. Li, L. Laguerre, B. Heritier, N. Benjelloun, M. Kadi, 2013. Determination of the compaction of hot mix asphalt using high-frequency electromagnetic methods. NDT & E International 60, 40–51.

[11]. S. Lambot, E. C. Slob, I. van den Bosch, B. Stockbroeckx and M. Vanclooster, "Modeling of ground-penetrating Radar for accurate characterization of subsurface electric properties," in Geoscience and Remote Sensing, IEEE Transactions on , vol.42, no.11, pp.2555-2568, Nov. 2004

[12]. S. Lambot, S. and F. André, "Full-Wave Modeling of Near-Field Radar Data for Planar Layered Media Reconstruction," Geoscience and Remote Sensing, IEEE Transactions on , vol.52, no.5, pp.2295,2303, May 2014

[13]. F. André and S. Lambot, "Intrinsic Modeling of Near-Field Electromagnetic Induction Antennas for Layered Medium Characterization," Geoscience and Remote Sensing, IEEE Transactions on , vol.52, no.11, pp.7457,7469, Nov. 2014

[14]. A. P. Tran and S. Lambot, "Intrinsic modeling of antenna array in near-field conditions," Ground Penetrating Radar (GPR), 2014 15th International Conference on GPR, vol., no., pp.519,524, June 30 2014-July 4 2014

[15]. C. Fauchard, B. Beaucamp, and L. Laguerre, “Non-destructive assessment of hot mix asphalt compaction/ density with a step-frequency radar: case study on a newly paved road,” Near Surface Geophysics, 13(2068), 2015

[16]. A. Kalogeropoulos, J. van der Kruk, J. Hugenschmidt, J. Bikowski and E. Brühwiler, “Full-waveform GPR inversion to assess chloride gradients in concrete,” NDT & E International, Volume 57, pp. 1-84, 2013

[17]. A. Ihamouten, G. Villain, G. and X. Derobert, "Complex Permittivity Frequency Variations From Multioffset GPR Data: Hydraulic Concrete Characterization," in Instrumentation and Measurement, IEEE Transactions on , vol.61, no.6, pp.1636-1648, June 2012

[18]. C. Le Bastard, Y. Wang, V. Baltazart and X. Dérobert, "Time Delay and Permittivity Estimation by Ground-Penetrating Radar With Support Vector Regression," in IEEE Geoscience and Remote Sensing Letters, vol. 11, no. 4, pp. 873-877, April 2014

[19]. J. Van der Kruk, A. Kalogeropoulos, J. Hugenschmidt, A. Klotzsche, S. Busch, H. Vereecken, “Full-waveform inversion of GPR data for civil engineering applications,” Geophysical Research Abstracts, Vol. 16, EGU2014-16051, 2014

[20]. A. P. Tran, F. André, C. Craeye, and S. Lambot, "Near-field or far-field full-wave ground penetrating radar modeling as a function of the antenna height above a planar layered medium," Progress In Electromagnetics Research, Vol. 141, 415-430, 2013

[21]. Reid A. Vilbig, " Air-coupled and ground-coupled ground penetrating radar technique", PhD thesis, 2013

513 [22]. S. Lambot, Method and device for characterization of physical properties of a target
514 volume by electromagnetic inspection, Patent EP2506040 A1, 2012

515 [23]. G. Villain and M. Thiery, "Gammadensimetry: A method to determine drying and
516 carbonation profiles in concrete, " NDT & E International, Volume 39, pp. 328 – 337, 2006

517 [24]. A. Ihamouten, K. Chahine, V. Baltazart, G. Villain, X. Derobert, "On Variants of the
518 Frequency Power Law for the Electromagnetic Characterization of Hydraulic Concrete," in
519 Instrumentation and Measurement, IEEE Transactions on, vol.60, no.11, pp.3658-3668, Nov.
520 2011

521 [25]. A.K. Jonscher, Dielectric Relaxation in Solids, London, U,K,: Chelsea Dielectrics
522 Press, 1983

523 [26]. S. Lambot, E. Slob, and H. Vereecken, (2007). Fast evaluation of zero-offset Green's
524 function for layered media with application to ground-penetrating radar. Geophysical
525 Research Letters 34, L21405, doi: 21410.21029/22007GL031459.

526 [27]. O. Lopera, E. Slob, N. Milisavljevic, and S. Lambot, (2007). Filtering soil surface and
527 antenna effects from GPR data to enhance landmine detection. IEEE Transactions on
528 Geoscience and Remote Sensing 45(3), 707-717.

529 [28]. X. Dérobert, C. Fauchard, P. Côte, E. Le Brusq, E. Guillanton, J. Y. Dauvignac, and
530 C. Pichot. Step-frequency radar applied on thin road layers. Journal of Applied Geophysics,
531 47(3–4) :317–325, 2001.

532